Diffuse optical monitoring of blood flow and oxygenation in human breast cancer during early stages of neoadjuvant chemotherapy

Chao Zhou
Regine Choe
University of Pennsylvania
Department of Physics & Astronomy
Philadelphia, Pennsylvania 19104

Natasha Shah
University of California
Beckman Laser Institute and Medical Clinic
Laser Microbeam and Medical Program
Irvine, California 92612

Turgut Durduran
University of Pennsylvania
Department of Physics & Astronomy and
    Department of Radiology
Philadelphia, Pennsylvania 19104

Guoqiang Yu
University of Pennsylvania
Department of Physics & Astronomy
Philadelphia, Pennsylvania 19104

Amanda Durkin
University of California
Beckman Laser Institute and Medical Clinic
Laser Microbeam and Medical Program
Irvine, California 92612

David Hsiang
Rita Mehta
John Butler
University of California
Chao Family Comprehensive Cancer Center
Irvine, California 92612

Albert Cerussi
Bruce J. Tromberg
University of California
Beckman Laser Institute and Medical Clinic
Laser Microbeam and Medical Program
Irvine, California 92612

Arjun G. Yodh
University of Pennsylvania
Department of Physics & Astronomy
Philadelphia, Pennsylvania 19104

Abstract. We combine diffuse optical spectroscopy (DOS) and diffuse correlation spectroscopy (DCS) to noninvasively monitor early hemodynamic response to neoadjuvant chemotherapy in a breast cancer patient. The potential for early treatment monitoring is demonstrated. Within the first week of treatment (day 7) DOS revealed significant changes in tumor/normal contrast compared to pretreatment (day 0) tissue concentrations of deoxyhemoglobin ($rctHHb_{T/N} = 69 \pm 21\%$), oxyhemoglobin ($rctO_2Hb_{T/N} = 73 \pm 25\%$), total hemoglobin ($rctTHb_{T/N} = 72 \pm 17\%$), and lipid concentration ($rctLipid_{T/N} = 116 \pm 13\%$). Similarly, DCS found significant changes in tumor/normal blood flow contrast ($rBF_{T/N} = 75 \pm 7\%$ on day 7 with respect to day 0). Our observations suggest the combination of DCS and DOS enhances treatment monitoring compared to either technique alone. The hybrid approach also enables construction of indices reflecting tissue metabolic rate of oxygen, which may provide new insights about therapy mechanisms. © *2007 Society of Photo-Optical Instrumentation Engineers.* [DOI: 10.1117/1.2798595]

Keywords: breast cancer; diffuse correlation spectroscopy; blood flow; diffuse optical spectroscopy; neoadjuvant chemotherapy; early monitoring; oxygen metabolism.

1 Introduction

Near-infrared (NIR) diffuse optical spectroscopy (DOS) and tomography (DOT) have been employed quantitatively by several groups to characterize breast cancers.[1–10] In clinical investigations, DOS and DOT have revealed tumor contrast in total hemoglobin concentration,[1,4,6–9,11–17] hemoglobin oxygen saturation,[4,11,12,14,17] water and lipid concentration,[14,17,18] and tissue scattering.[2,16,18] Furthermore, DOS and DOT have also shown promise for therapeutic monitoring of breast cancer

patients.[14–17,19,20] Studies during neoadjuvant chemotherapy (chemotherapy prior to surgery) have shown that tumor metabolic response can precede anatomical changes (e.g., size) accessible to traditional imaging and clinical palpation methods.[21] Thus, new diagnostic methodologies focusing on physiological properties of the tumor, for example, hemodynamic response, may offer benefits beyond those of traditional imaging and palpation during the early course of chemotherapy. In a recent case study, for example, Jakubowski et al.[14] used DOS and observed significant changes in total

Address all correspondence to: Chao Zhou, University of Pennsylvania, Department of Physics & Astronomy, 209 S. 33rd St., Philadelphia, PA, 19104; Tel: 215-898-8422; Fax: 215-573-6391; E-mail: chaozhou@alumni.upenn.edu

hemoglobin concentration and water fraction within 5 days of the start of treatment.

Another important hemodynamic parameter is blood flow. Measurements of blood flow provide insight about oxygen delivery and the clearance of metabolic by-products, complementary to information about tissue chromophores and scattering available to DOS. *In vivo* diffuse optical measurement of blood flow has recently been explored using diffuse correlation spectroscopy[22–25] (DCS) in brain,[26–31] muscle,[32,33] and in the tumor tissues[34–37] of animal models and humans. A recent DCS study in human breast tumors[37] showed increased blood flow contrast in tumor regions relative to adjacent healthy tissue, consistent with results from ultrasound,[38] positron emission tomography[39] (PET), and magnetic resonance imaging[40] (MRI). In some cases, the DCS technique has been validated[33,34] with ultrasound and MRI, and in a few cases the therapy monitoring capability of hybrid DCS/DOS instruments has been demonstrated.[34–36] The latter instruments are particularly exciting because, in principle, the oxygen delivery information derived from blood flow can be used in combination with blood oxygenation measurements to estimate the metabolic rate of oxygen consumption in tissue.

In this paper, we describe a case study of a breast cancer patient during the early stages of neoadjuvant chemotherapy. In contrast to previous optical measurements of breast tumors, the current work used both DOS and DCS in the same patient to derive information about tumor chromophores, tumor scattering, and tumor blood flow. Significant changes in tissue hemodynamic parameters were detected as early as 3 days post-therapy. To date, several studies have focused on measurements of parameters related to cancer metabolism and blood flow after few cycles of chemotherapy, i.e., after several weeks.[39,41–45] The present study has focused on daily measurements within the first week. The observations of blood flow changes are the first of their kind during early stage chemotherapy. The combined DOS/DCS information provides a more complete picture of tumor tissue hemodynamics and enables us to construct new indices reflecting changes in oxygen metabolism that require knowledge about flow and oxy- and/or deoxyhemoglobin concentrations.

2 Materials and Methods

2.1 Protocol

The patient measurements were conducted at the Beckman Laser Institute of the University of California, Irvine (UCI), and were approved by the Internal Review Board at UCI. The subject was a 45-year-old premenopausal Caucasian woman undergoing neoadjuvant chemotherapy treatment; she provided informed written consent for Human Subjects protocol 95-563. The patient was diagnosed by core biopsy revealing invasive ductal carcinoma in the left breast. Clinical palpation identified an 11-cm × 5-cm area at 3 o'clock [Fig. 1(a)]. Dynamic contrast-enhanced MRI (DCE-MRI) detected several strongly enhanced masses within this area. The outer edge of the tumor was located 0.5 to 1 cm underneath the skin. In addition, the patient had multiple benign lesions at 1 o'clock (by ultrasound). The tumor position was identified by palpation and ultrasound and was marked with a surgical pen to ensure the scans on different days were performed at the same location. The surgical pen marks were visible after day 3, and
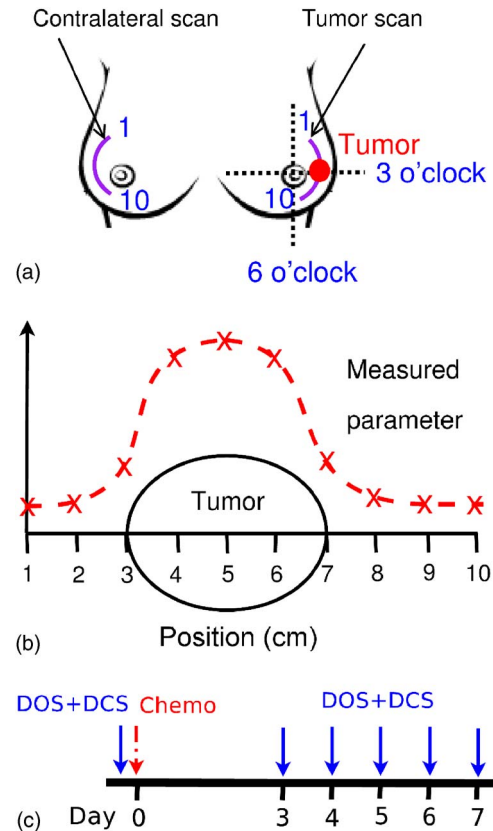

Fig. 1 (a) Tumor position and line-scan directions. Starting from point 1 in the upper outer quadrant, optical measurements were performed at 1-cm intervals, ending at point 10 in the lower outer quadrant. (b) Illustration of the line scans over the tumor. (c) Timing diagram for chemotherapy monitoring.

they were redrawn every day afterward. The accuracy for redrawing was within 2 to 3 mm. The optical probe repositioning accuracy was of similar order (i.e., 2 to 3 mm). Measurements were made with the patient in the supine position. DOS and DCS measurements were acquired using handheld probes at 10 discrete points in a line along the curved surface at 1-cm intervals across the tumor and surrounding tissue ("line scan"). The same measurement pattern was used on the contralateral breast for comparison. Figures 1(a) and 1(b) show the tumor position and line-scan directions on the patient, where the tumor center was located at the 5-cm position. One line scan took about 10 (8) min per breast for DOS (DCS), respectively, resulting in a measurement time of about 40 min per session. Extra care was taken during the DCS measurement to gently press the probe on the patient's breast; the operator attempted to keep that pressure relatively constant and the probe stable.

The patient was treated with neoadjuvant chemotherapy delivered in multiple stages. The initial treatment stage consisted of doxorubicin (Adriamycin) and cyclophosphamide (Cytoxan, A/C) therapy. A/C treatments were administered once per cycle for four cycles, with each cycle lasting 2 weeks. Doxorubicin is a cytoxic anthracycline antibiotic, and its mechanism of action is thought to prevent DNA and possibly RNA synthesis by intercalation. Doxorubicin was administered at a dose of 60 mg/m^2 once per cycle. Cyclophos-

phamide is biotransformed principally in the liver to activate alkylating metabolites, which cross-link to tumor cell DNA. Cyclophosphamide was administered at a dose of 600 mg/m^2 once per cycle. DOS and DCS measurements were performed on the same day prior to the therapy (day 0), and every day between 3 to 7 days after the first A/C cycle [day 3 to day 7, Fig. 1(c)]. Additional stages using other therapies were administered, but no DOS/DCS measurements were recorded during these treatment stages (DOS/DCS measurements ended on day 7). The most relevant radiologic assessment was the DCE-MRI study done 12 days after the first A/C therapy, which showed shrinkage of multiple lesions, the largest lesion of which shrunk by 1.7 cm (in diameter). Ultrasound measurements were performed after the completion of all four A/C cycles (8 weeks) and detected an irregular hypoechoic lesion of 1.3 cm in diameter, indicating a partial response to A/C therapy. At the end of chemotherapy, DCE-MRI showed several tiny enhanced foci. The surgical pathology from lumpectomy at the conclusion of chemotherapy revealed residual intraductal and invasive ductal carcinoma with extensive fibrosis.

2.2 Instrumentation

2.2.1 DOS

A broadband DOS system developed[46] at UCI was utilized to determine tissue optical properties and tissue blood oxygenation *in vivo*. The system combined a steady state (SS) tungsten-halogen light source and spectrophotometer operating in the 600 to 1000-nm range and a frequency-domain photon migration (FDPM) component (based on a network analyzer) consisting of six laser diodes (operating at discrete wavelengths in the 660 to 850-nm range). The combination of the cw and discrete spectral components enabled determination of complete μ_a and μ_s' spectra from 600 to 1000 nm. Measurements were made using a handheld probe consisting of the SS and FDPM source fibers, one avalanche photodiode (APD) detector and one spectrometer detector fiber. The source-detector separation was 2.8 cm and the time to perform SS and FDPM measurements at a single position was typically about 30 to 45 s. A detailed description of the performance of this device in 58 breast cancer patients has recently been reported.[10]

2.2.2 DCS

A portable two-channel DCS instrument ($18 \times 28 \times 33$ cm) was built at the University of Pennsylvania and transported to UCI for the measurements of blood flow. Briefly, a compact cw 785-nm long coherence laser (coherence length ~50 m, Crystalaser, Reno, Nevada) was used as the light source. Two fast-photon-counting APDs (Perkin-Elmer, Canada) were used to register the photons collected with single-mode fibers. A custom-built two-channel correlator board (www.correlator .com, New Jersey) took the transistor-to-transistor logic (TTL) output from the APDs and calculated normalized temporal intensity autocorrelation functions of the detected light, $g_2(\tau) = \langle I(t)I(t+\tau)\rangle/\langle I(t)\rangle^2$, where $I(t)$ is the measured intensity at time t, τ is the correlation delay time, and the angle brackets $\langle\rangle$ denote an average over time. A single source fiber and two detector fibers were used in the handheld probe with 2.5-cm source-detector separations. Thus, the DCS measure-

ment probed approximately the same volume of breast tissue as the DOS measurement and a typical photon count rate of ~30 kHz was obtained from the breast measurement. Each temporal autocorrelation curve was averaged for 2.5 s, and multiple DCS measurements (typically >10) were performed at a single position to ensure a good signal-to-noise ratio (SNR).

2.3 Data Analysis

2.3.1 DOS Measurements

The algorithm for analyzing the DOS data was described in detail by Bevilacqua et al.[46] Briefly, the frequency domain measurements at six discrete wavelengths were used to extract the reduced scattering coefficient (μ_s') at each wavelength. A power law function,[47–49] $\mu_s'(\lambda) = A\lambda^{-b}$, was then fit to the wavelength-dependent μ_s' to estimate the scattering information at all other wavelengths. With $\mu_s'(\lambda)$ input from the frequency-domain measurements, the data measured with the spectrometer system was employed to extract accurate absorption coefficients $\mu_a'(\lambda)$ over the whole spectral range. As a result, tissue concentrations of oxy-, deoxy-, and total hemoglobin (ctO$_2$Hb, ctHHb and ctTHb), water (ctH$_2$O) and lipid (ctLipid) were reconstructed by decomposing the absorption spectra.[46] Note that our notation is designed to comply with Zander and Mertzlufft,[50] where the prefix "ct" indicates tissue-level concentration (see Table1).

2.3.2 DCS Measurements

We used the intensity temporal autocorrelation curves measured with the DCS instrument to extract tissue blood flow information. The decay rate of the correlation curves is correlated with the blood flow, e.g., faster decay reflects higher blood flow. In our analysis, the photon correlation diffusion equation[24,25] was used to model the propagation of the electric field autocorrelation function, $G_1(\mathbf{r}, \tau) = \langle E(\mathbf{r}, t)E^*(\mathbf{r}, t+\tau)\rangle$, inside tissues,

$$\nabla[D \nabla G_1(\mathbf{r}, \tau)] - \left[v\mu_a' + \frac{1}{3}v\mu_s'\mathbf{k}_0^2\alpha\langle\Delta r^2(\tau)\rangle \right] G_1(\mathbf{r}, \tau) =$$
$$-vS\delta^3(\mathbf{r} - \mathbf{r}_s). \tag{1}$$

Here, $E(\mathbf{r}, t)$ is the electric field at position $\mathbf{r}$ and time t, τ is the correlation delay time, v is the light speed in the media, D $v/3\mu_s'$ is the light diffusion constant, k_0 is the optical wave vector, $\langle\Delta r^2(\tau)\rangle$ is the mean-square displacement of the moving scatters in time τ, and $S\delta^3(\mathbf{r} - \mathbf{r}_s)$ is the point source term located at $\mathbf{r}_s$. The normalized electric field autocorrelation function $g_1(\mathbf{r}, \tau) = G_1(\mathbf{r}, \tau)/G_1(\mathbf{r}, 0)$ is related to the measured intensity autocorrelation function $g_2(\mathbf{r}, \tau)$ through the Siegert relation[51]:

$$g_2(\mathbf{r}, \tau) = 1 + |g_1(\mathbf{r}, \tau)|^2, \tag{2}$$

where depends on the detection optics (e.g., it is inversely proportional to the number of detected speckles). We determined for each measurement. The decay of the correlation function depends on tissue μ_a and μ_s', the mean square displacement $\langle\Delta r^2(\tau)\rangle$, of the moving scatterers inside the tissue, and a unitless factor α that represents the fraction of scatterers

Table 1 Table of abbreviations.

Name	Symbol	Units
Deoxy-hemoglobin concentration	ctHHb	μM
Oxy-hemoglobin concentration	ctO$_2$Hb	μM
Total hemoglobin concentration	ctTHb	μM
Hemoglobin oxygen saturation	stO$_2$	%
Water concentration	ctH$_2$O	% (with respect to pure substance)
Lipid concentration	ctLipid	% (with respect to pure substance)
Blood flow index	BFI	cm^2/s
Tissue optical index	TOI	μM
Mammary metabolic rate of oxygen	MMRO$_2$	μM/100 g min^{-1}
Tumor/normal contrast	T/N	folds
Relative change compared to day 0	r	%

Notes on nomenclature: (1) a prefix ct indicates tissue-level concentration of the parameter; (2) subscripts T and N indicate values of tumor and normal tissues, respectively, where a subscript T/N indicates the tumor/normal contrast; (3) a prefix r indicates relative change compared to prechemotherapy value (day 0).

that are moving (i.e., red blood cells). A semi-infinite solution to Eq. (1) (Ref. 25) was used in our data analysis. We have observed that a diffusion model, i.e., $\langle \Delta r^2(\tau) \rangle = 6D_b\tau$, fits the autocorrelation curves rather well over a broad range of tissue types, including the present experiments.[26,32,34,52] Here, D_b is the *effective* Brownian motion coefficient of the scatterers (distinct from the well known thermal Brownian motion coefficient due originally to Einstein[53]). Although the units of αD_b (square centimeters per second) is different from the traditional blood perfusion unit (milliliters per minute per 100 g), we have verified that changes in αD_b are proportional to the changes in tissue blood flow in a wide range of measurements.[32–34,52,54] Determination of α is difficult. Therefore in the current study, we report αD_b as the blood flow index (BFI$= \alpha D_b$). Bulk optical properties of the breast, μ_a and μ_s' at 785 nm, were obtained from the DOS measurements and used in the DCS data analysis to minimize the influence of optical property changes on the accuracy of BFI. In our fitting process, the noise in the correlation curve (τ) was estimated as a function of delay time τ, and was used in calculating ^{2}, e.g., $^2 = g_{2m}(\tau) - g_{2c}(\tau)/ (\tau)\|$, where $g_{2m}(\tau)$ and $g_{2c}(\tau)$ are the measured and calculated intensity autocorrelation curves, respectively. A more stable BFI is usually obtained from the fitting by minimizing ^{2} as defined in this way.[30]

2.3.3 Tissue Optical Index

The tissue optical index (TOI) is a multiparameter contrast function created to maximize both the contrast and the specificity of the optical measurement. The TOI is defined as[10,19]

$$TOI = \frac{ctHHb \cdot ctH_2O}{ctLipid}. \qquad (3)$$

The parameters in this contrast function were chosen based on a statistical study of 58 malignant breast lesions.[10] In this study, deoxy-hemoglobin was identified as the single best discriminator between malignant tumors and normal tissue, and it was found that addition of water and lipid concentrations further improved malignant/normal discrimination. The simplest index combining these parameters used ctHHb and ctH$_2$O in the numerator and ctLipid in the denominator. As such, increased TOI reflects a higher chance of tumor malignancy. Conceptually, the TOI takes into account functional (ctHHb and ctH$_2$O) and structural (ctLipid and ctH$_2$O) information. TOI is also related to metabolic activity since increases in deoxy-hemoglobin are often a symptom of unmet metabolic demand.

2.3.4 Oxygen Metabolism

Another, and perhaps more direct, estimate of tissue oxygen metabolism can be calculated by combining information about blood flow (delivery of oxygen) measured by DCS with chromophore concentration information such as blood oxygen saturation (i.e., oxygen availability) measured by DOS. This approach is often employed in studies of cerebral metabolic rate of oxygen[55–60] (CMRO$_2$). In the simplest model, CMRO$_2$ is proportional to the tissue arterial-venous oxygenation difference or oxygen extraction fraction (OEF) as well as the rate of oxygen delivery (i.e., the cerebral blood flow, CBF). Several assumptions are typically made in the steady-state model, including constant vasculature compartmentalization. The CMRO$_2$ model has been fairly well studied, validated and its limits examined.[27,28,55–61]

In this paper, we construct a mammary oxygen metabolism model that closely follows the CMRO$_2$ approach in brain (see the appendix). We define the tumor/normal contrast of the mammary metabolic rate of oxygen (MMRO$_{2(T/N)}$) as,

$$\text{MMRO}_{2(T/N)} = \frac{\Gamma_T}{\Gamma_N} \cdot \frac{\text{ctHHb}_T}{\text{ctHHb}_N} \cdot \left(\frac{\text{ctTHb}_T}{\text{ctTHb}_N} \right)^{-1} \cdot \frac{\text{BFI}_T}{\text{BFI}_N}, \quad (4)$$

where T and N represent the values for tumor and normal breast tissue (i.e., normal tissues within the same breast), and $\Gamma_{T(N)} = [\text{ctHHb}_{vT(N)}/\text{ctTHb}_{vT(N)}]/[\text{ctHHb}_{T(N)}/\text{ctTHb}_{T(N)}]$ is the ratio of tumor (or normal) deoxy-to total-hemoglobin in the venous compartment (v) compared to the ratio of deoxy-to total-hemoglobin in the total vasculature (see the appendix). The simplest approximation, which we adopt here, assumes the ratio of Γ_T/Γ_N to be 1 and constant over time. The relative tumor/normal contrast of mammary metabolic rate of oxygen (rMMRO$_{2(T/N)}$, see Table 1) can now be estimated from our measurements. We note, however, that these assumptions are unverified. The precise quantification of Γ_T and Γ_N requires better understanding of the microcirculation in tumor and normal tissues, and such precision is beyond the scope of the current study.

2.3.5 *Characterization of Responses*

To quantify tumor response to chemotherapy, the tumor/normal contrast for the parameters at each time point was determined. Tumor/normal contrast was calculated as the ratio of the average tumor value (positions 3 to 7 in the line scans) to the average value of the normal tissue on the same side of the breast (i.e., positions 8 to 10), for example, BF$_{T/N}$ = BFI$_T$/BFI$_N$, ctTHb$_{T/N}$=ctTHb$_T$/ctTHb$_N$, etc. The positions were chosen based on palpation, and positions 1 and 2 were excluded as normal tissue because they were too close to other benign lesions. This calculation effectively accounts for the global variations in response to chemotherapy by normalizing to the daily normal tissue values. Thus, the tumor specific responses of each parameter are "pulled" out of the measurement. The tumor/normal contrast for each time point was then normalized to prechemotherapy values (day 0) to reflect relative changes, indicated by a prefix "r" for each parameter (see Table 1). Wilcoxon rank-sum tests were conducted comparing the optically measured differences between tumor and normal on day 0. Significant changes were observed and marked in the figures with an '*', representing a significance level of $p < 0.05$ compared to prechemotherapy values.

3 Results and Discussion

Figure 2 exhibits representative DCS temporal autocorrelation curves measured on the tumor before and after the first A/C treatment (days 0, 3, and 7). The figure also shows data from normal tissue from both breasts on day 0. The symbols are raw data and the solid lines are fitted curves. The correlation curves measured on the tumor have significantly faster decay rates compared to those from normal breast tissues, indicating higher blood flow in the tumor. The measurements from the tumor on different days are clearly distinguishable from one another with good SNR, thus enabling us to quantify tumor blood flow changes due to chemotherapy.

Figure 3 shows line scans of blood flow index [BFI $= \alpha D_b$, Fig. 3(a)] and total hemoglobin concentration [ctTHb, Fig. 3(b)] from both the tumor breast and the contralateral breast before and after the first chemotherapy treatment (days 0, 3, and 7). Error bars in the figures represent the standard deviation of repeated measurements. The measurements con-
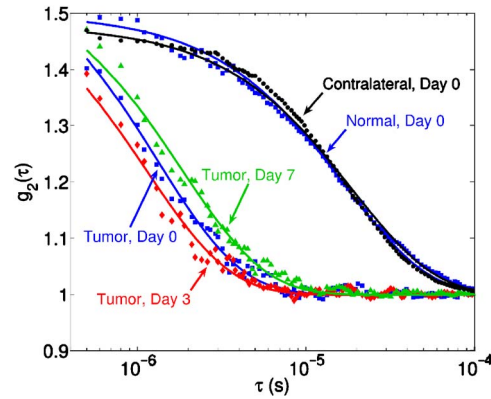

Fig. 2 Raw (symbols) and fitted intensity autocorrelation curves (solid lines) measured from the patient before and after chemotherapy (day 0, day 3, and day 7). Both Γ and the BFI (BFI$=\alpha D_b$) were fit. Similar Γ values were obtained for both normal and tumor breast tissues. The correlation curves measured on the tumor have larger decay rates compared to the curves measured on the contralateral breast, indicating higher blood flow in the tumor.

ducted on different days were reproducible, which can be seen from the scans on the contralateral breast and the normal tissues on the tumor-bearing breast (positions 8 to 10). BFI exhibited significant increases in the tumor breast (i.e., 10.6 ± 1.8 folds) relative to the heterogeneity of normal breast tissue on the contralateral side (i.e., 2.1 ± 0.7). ctTHb also showed clear tumor/normal contrast (i.e., 2.1 ± 0.3). For clarity, line–scans for other hemodynamic parameters, such as ctHHb, ctO$_2$Hb, and water and lipid concentrations, are not plotted. The observed tumor/normal contrast of these parameters is consistent with previous reports,[10,14] i.e., ctHHb had a contrast of 2.1 ± 0.2, ctO$_2$Hb had a contrast of 2.0 ± 0.3, water had a contrast of 1.9 ± 0.3, ctLipid had a contrast of 0.8 ± 0.05, and μ_s' at 785 nm had a contrast of 0.96 ± 0.03 prior to the A/C treatment.

Neoadjuvant chemotherapy can induce hemodynamic changes in both tumor and normal tissues.[14,16] To investigate the tumor specific changes in response to the chemotherapy, relative tumor/normal contrast of ctHHb, ctO$_2$Hb, and ctTHb with respect to pretherapy values (rctHHb$_{T/N}$, rctO$_2$Hb$_{T/N}$, and rctTHb$_{T/N}$) were calculated and are plotted in Fig. 4. Notice that significant changes in these hemodynamic parameters were observed as early as 4 days after the start of A/C therapy ($p < 0.05$), i.e. rctHHb$_{T/N}$ dropped to $68 \pm 12\%$ of its original value (day 0); rctO$_2$Hb$_{T/N}$ dropped to $63 \pm 10\%$; and rctTHb$_{T/N}$ dropped to $63 \pm 10\%$. By the end of the monitoring period (day 7), there were continued small hemodynamic reductions and all values remained substantially lower than pretreatment levels (day 0): rctHHb$_{T/N}$ dropped to $69 \pm 21\%$ ($p < 0.05$); rctO$_2$Hb$_{T/N}$ dropped to $73 \pm 25\%$ ($p < 0.05$); and rctTHb$_{T/N}$ dropped to $72 \pm 17\%$ ($p < 0.05$).

Relative tumor/normal contrast of blood flow (rBF$_{T/N}$), concentration of water (rctH$_2$O$_{T/N}$) and lipid (rctLipid$_{T/N}$), and reduced scattering coefficient $[r\mu_{s(T/N)}']$ in response to the chemotherapy are plotted in Fig. 5. Blood flow measured with DCS showed good SNR ratio and substantial tumor-to-normal contrast. rBF$_{T/N}$ increased initially on day 3 after the A/C therapy ($130 \pm 13\%, p < 0.05$), followed by a sharp and sus-
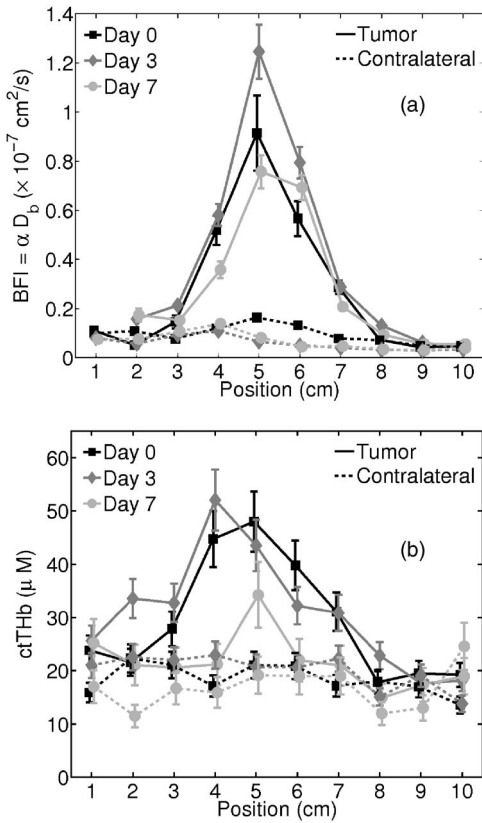
Fig. 3 Line scans of (a) BFI and (b) ctTHb before and after the first chemotherapy cycle (day 0, day 3, and day 7). On the tumor side of the breast, BFI showed clear contrast, which was much larger than the heterogeneity of the breast tissue on the contralateral side. The ctTHb also showed clear contrast on the tumor. Tumor contrasts changed in response to the chemotherapy. For clarity, line scans of other hemodynamic parameters, such as ctHHb, ctO$_2$Hb, and water and lipid concentrations, are not plotted. Error bars represent the standard deviation of repeated measurements. Plots were slightly offset along the x axis for better illustration of the error bars.

Fig. 4 Relative tumor/normal ctHHb, ctO$_2$Hb, and ctTHb contrast (rctHHb$_{T/N}$, rctO$_2$Hb$_{T/N}$ and rctTHb$_{T/N}$) in response to chemotherapy. The contrasts were calculated as the ratio of the average tumor value (positions 3 to 7 in the line scans) to the average value of the normal tissue on the same side of the breast (positions 8 to 10). The contrasts were then normalized to the pre-chemotherapy values to reflect relative changes. Significant decreases in the contrast occurred in all three parameters 4 days after the chemotherapy. Asterisks (*) denote the data points significantly different from the pre-chemotherapy values (day 0, p 0.05). Plots were slightly offset along the x axis for better illustration of the error bars.

of fiber optics could have an effect on our DCS measurements. In a previous experiment,[32] we have carried out tests that suggest the movement of fiber optics do not influence the DCS measurements after the optical probe was secured in place. An indication that the pressure and motion effects are minimal can be seen from the relatively small variations measured on the contralateral side of the breast (Fig. 3), i.e., the
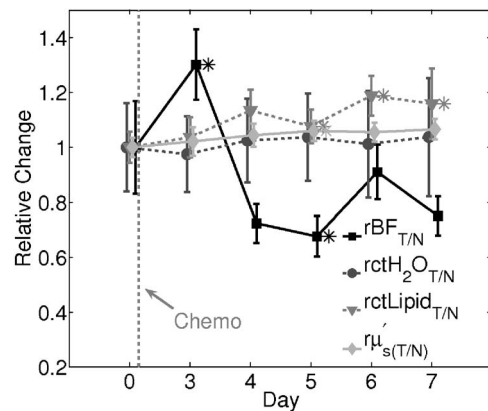
Fig. 5 Relative tumor/normal blood flow index, water, lipid and μ'_s contrast (rBF$_{T/N}$, rctH$_2$O$_{T/N}$, rctLipid$_{T/N}$, and r$\mu'_{s(T/N)}$) in response to chemotherapy. The contrasts were calculated as the ratio of the average tumor value (positions 3 to 7 in the line scans) to the average value of the normal tissue on the same side of the breast (positions 8 to 10). The contrasts were then normalized to the pre-chemotherapy values to reflect relative changes. rBF$_{T/N}$ showed an significant initial increase (p 0.05) on day 3 and a significant decrease on day 5 (p 0.05). Water contrast did not change significantly in response to the chemotherapy, while lipid contrast increased significantly after day 5 (p 0.05). Asterisks (*) denote the data points significantly different from the pre-chemotherapy values (day 0, p 0.05). Plots were slightly offset along the x axis for better illustration of the error bars.

tained drop on days 4 ($72 \pm 7\%, p=0.13$), 5 ($68 \pm 7\%, p$ 0.05), and 7 ($75 \pm 7\%, p=0.13$). rctLipid$_{T/N}$ increased significantly from day 5 ($108 \pm 6\%, p$ 0.05) to day 7 ($116 \pm 13\%, p$ 0.05). Since the lipid concentration in tumor was lower than in the normal breast tissues before the therapy, the increase in rctLipid$_{T/N}$ suggests that lipid concentration in the tumor is normalized over time. The $r\mu'_{s(T/N)}$ at 785 nm had a small increase within the week (7%, $p>0.05$), despite the increase on day 5, which was significant ($106 \pm 4\%, p$ 0.05). No significant changes for the relative contrast of water concentration (rctH$_2$O$_{T/N}$) were observed within the first week. However, the subject was also enrolled in a separate study for DOS, wherein significant decrease in water contrast was observed after 4 months (i.e., rctH$_2$O$_{T/N}$ decreased to $68 \pm 7\%, p$ 0.01).

Note, the optical properties (μ_a and μ'_s) of the breast tissue at 785 nm were measured by the DOS instrument. Measured absorption and scattering effects are incorporated into the DCS data analysis. As a result, the influence of oxygenation state of the breast should not influence our blood flow results. On the other hand, probe contact pressure and the movement
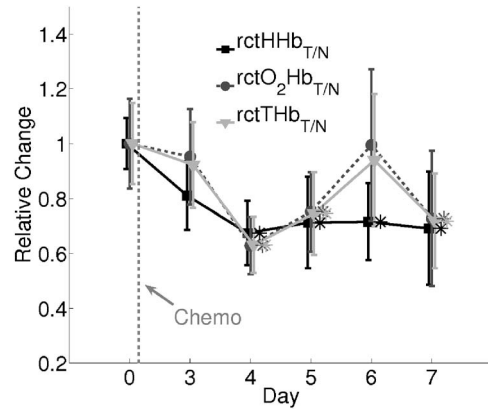
day-to-day tumor contrast and variation were large compared to the combination of measurement noise, physiological noise, motion artifact noise, and pressure related variations experienced on the contralateral breast.

Chemotherapy treatment alters tumor angiogenesis.[62] Therefore, optical properties of the tumor are expected to change due to chemotherapy, which is observed in our measurements. Although chemotherapy may also induce changes of other kinds of microscopic motions inside the tumor, we believe such an effect is likely small compared to the changes in tumor vasculature and blood flow. In our previous study of photodynamic therapy treatment of mouse tumors,[34] blood flow changes measured with both ultrasound Doppler and DCS showed comparable results, indicating the tumor responses measured with DCS are mainly due to blood flow. The relative tumor blood flow reduction in response to neoadjuvant chemotherapy observed in the current study ($\sim$25% within the first week) is also consistent with results from PET studies,[39,63] wherein a 30% to 50% blood flow decrease after 2 months of chemotherapy was reported. Yet blood flow changes exhibit distinct features compared to other hemodynamic parameters measured with DOS. For example, we have observed an $\sim$30% initial increase in $rBF_{T/N}$ on day 3 in this patient (Fig. 5), accompanied by an $\sim$20% decrease in $rctHHb_{T/N}$ (Fig. 4). Although the mechanism is not clear, this may be due to an early tumor vascular response to cellular damage. The $\sim$20% decrease in $rctHHb_{T/N}$ on day 3 could be consistent with reduced oxygen extraction given that $rctTHb_{T/N}$ remained roughly constant and flow was elevated. By day 4, A/C therapy has continued to damage both cells and vasculature; $rBF_{T/N}$, $rctHHb_{T/N}$, and $rctHHb_{T/N}$ all decreased because of significant damage to tumor cells. A similar initial increase followed by a significant decrease of blood flow was observed during the first few days after radiation therapy in patients with breast tumors.[64] In patients with head and neck tumors,[36,65] and rectal carcinoma,[66] similar patterns of blood flow changes were also reported in the early weeks after radiation therapy. Further studies involving more patients are underway to confirm the observations in this case study.

As described in Sec. 2.3, the combination of DCS and DOS measurements enable oxygen metabolic changes in the tumor to be calculated using Eq. (4). Compared to flow, hemoglobin concentrations, and other tissue parameters alone, this relative metabolism index is a potentially more direct indicator of tumor metabolic activities that integrates many factors and may provide further insight about tumor physiological responses to therapy. Figure 6 displays the relative changes in tumor/normal contrast of mammary metabolic rate of oxygen and the tissue optical index based on chromophore concentrations [i.e., $rMMRO_{2(T/N)}$ and $rTOI_{T/N}$]. Values of relative tumor/normal contrast for all the optically derived parameters are listed in Table 2. $rMMRO_{2(T/N)}$ and $rTOI_{T/N}$ differed on day 3, e.g. $rTOI_{T/N}$ had an initial drop ($72\pm16\%$, $p=0.13$) and $rMMRO_{2(T/N)}$ had an initial increase ($118\pm13\%$, $p=0.68$), but both parameters were only marginally different from day 0. The initial increase observed in $rMMRO_{2(T/N)}$ is most probably a result of the initial increase of blood flow, although further evidence is needed for this hypothesis to be confirmed. However, after day 4, both metabolic indices dropped significantly ($rTOI_{T/N}=60\pm9\%$,
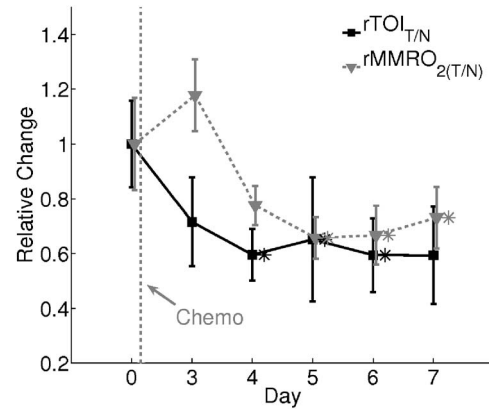

Fig. 6 Relative tumor/normal tissue optical index and mammary metabolic rate of oxygen contrast [$rTOI_{T/N}$ and $rMMRO_{2(T/N)}$] in response to chemotherapy. The contrasts were calculated as the ratio of the average tumor value (positions 3 to 7 in the line scans) to the average value of the normal tissue on the same side of the breast (positions 8 to 10). The contrasts were then normalized to the prechemotherapy values to reflect relative changes. Significant decreases were observed in both $rTOI_{T/N}$ and $rMMRO_{2(T/N)}$ after day 4. Asterisks (*) denote the data points significantly different from the prechemotherapy values (day 0, p 0.05). Plots were slightly offset along the x axis for better illustration of the error bars.

p 0.05 and $rMMRO_{2(T/N)}=78\pm7\%$, p 0.05 on day 4) and then stabilized at this level until the end of the monitoring period. We note that although both $TOI_{T/N}$ and $MMRO_{2(T/N)}$ are considered to be related to tumor metabolic responses, $TOI_{T/N}$ provides information about tumor cellular metabolic activities,[19,67] while $MMRO_{2(T/N)}$ provides an estimation of tumor oxygen metabolic changes. Note that tumors have abnormal vasculatures and the input and output circulations to and from the tumor are not well characterized. Our assumption of $saO_{2T}=1$ (see the appendix) may not be true, but in the absence of more information, we believe this is a reasonable starting assumption. $MMRO_{2(T/N)}$ (Eq. (4)) functions more as a relative index of oxygen consumption than as a quantitative measure of true oxygen metabolism. We have introduced $MMRO_{2(T/N)}$ as a potentially useful index for monitoring cancer physiology accessible to the optical method. Its utility, however, must be determined by more clinical studies. To date only a few *in vivo* studies on human tumors have probed oxygen metabolism.[68–71] Further studies and validation in animal models using methods presented in this paper may be useful to improve the oxygen metabolism model in tumors, to reveal the connections between TOI and oxygen metabolism, and to provide potential diagnostics for chemotherapy efficacy.

4 Conclusion

We reported a case study wherein we monitored hemodynamic and tissue optical property changes in a breast tumor patient undergoing neoadjuvant chemotherapy. Our approach employed a combination of DOS and DCS to measure simultaneously blood oxygenation, lipid, water, and blood flow. We demonstrated the feasibility of this methodology and detected significant changes in tissue parameters as early as day 3 following the first chemotherapy infusion. This study introduced

Table 2 Tumor/normal contrast changes normalized to day 0 values of all parameters within the first week of chemotherapy.

	Day 0	Day 3	Day 4	Day 5	Day 6	Day 7
$rctHHb_{T/N}$	1.00 ± 0.09	0.81 ± 0.12	$0.68 \pm 0.12^*$	$0.71 \pm 0.17^*$	$0.72 \pm 0.14^*$	$0.69 \pm 0.21^*$
$rctO_2Hb_{T/N}$	1.00 ± 0.16	0.95 ± 0.17	$0.63 \pm 0.10^*$	$0.75 \pm 0.14^*$	1.00 ± 0.28	$0.73 \pm 0.25^*$
$rctTHb_{T/N}$	1.00 ± 0.15	0.92 ± 0.16	$0.63 \pm 0.10^*$	$0.75 \pm 0.15^*$	0.94 ± 0.24	$0.72 \pm 0.17^*$
$rctH_2O_{T/N}$	1.00 ± 0.16	0.97 ± 0.14	1.02 ± 0.15	1.04 ± 0.16	1.01 ± 0.19	1.04 ± 0.22
$rctLipid_{T/N}$	1.00 ± 0.06	1.04 ± 0.07	1.13 ± 0.08	$1.08 \pm 0.06^*$	$1.19 \pm 0.07^*$	$1.16 \pm 0.13^*$
$rBF_{T/N}$	1.00 ± 0.17	$1.30 \pm 0.13^*$	0.72 ± 0.07	$0.68 \pm 0.07^*$	0.91 ± 0.10	0.75 ± 0.07
$r\mu'_{s(T/N)}$	1.00 ± 0.03	1.02 ± 0.05	1.04 ± 0.04	$1.06 \pm 0.04^*$	1.06 ± 0.03	1.07 ± 0.04
$rTOI_{T/N}$	1.00 ± 0.16	0.72 ± 0.16	$0.60 \pm 0.09^*$	$0.65 \pm 0.23^*$	$0.59 \pm 0.13^*$	0.59 ± 0.18
$rMMRO_{2(T/N)}$	1.00 ± 0.17	1.18 ± 0.13	0.78 ± 0.07	$0.66 \pm 0.08^*$	$0.67 \pm 0.11^*$	$0.73 \pm 0.11^*$

Asterisks (*) denote the data points significantly different from the prechemo therapy values (day 0, p 0.05).

optical measurement of blood flow as a new parameter for therapy monitoring along with multiparameter indices that may provide further physiological insight, such as tissue metabolic rate of oxygen. Overall, the hybrid diffuse optical approach shows promise for therapy monitoring, optimization, and personalization by potentially detecting physiological changes that may precede anatomical changes accessible to traditional radiological diagnostics procedures.

Appendix

In this section, we derive the equation for the calculation of the tumor/normal contrast of the mammary metabolic rate of oxygen $[MMRO_{2(T/N)}]$ following the steps in deriving the cerebral metabolic rate of oxygen $(CMRO_2)$.[27,55–60]

Using Fick's law, the tumor (or normal) mammary metabolic rate of oxygen $[MMRO2T(N)]$ can be calculated as

$$MMRO_{2T(N)} = OEF_{T(N)} \cdot BF_{T(N)} \cdot [O_2]_{aT(N)}. \quad (5)$$

The tumor (or normal) oxygen extraction factor $[OEF_{T(N)}]$ is by definition the fractional conversion of oxygen from arterioles to venules, i.e., $OEF_{T(N)} = ([O_2]_{aT(N)} - [O_2]_{vT(N)})/[O_2]_{aT(N)}$, where $[O_2]_{aT(N)}$ and $[O_2]_{vT(N)}$ are the tumor (or normal) arteriolar and venous concentrations of oxygen. $BF_{T(N)}$ is the tumor (or normal) blood flow. In steady-state, assuming a balance between oxygen concentration and oxyhemoglobin saturation in the arteriolar and venous compartments $[saO_{2T(N)}$ and $svO_{2T(N)}]$, we have

$$\frac{OEF_T \cdot [O_2]_{aT}}{OEF_N \cdot [O_2]_{aN}} = \frac{[O_2]_{aT} - [O_2]_{vT}}{[O_2]_{aN} - [O_2]_{vN}} = \frac{saO_{2T} - svO_{2T}}{saO_{2N} - svO_{2N}}. \quad (6)$$

As a result, the tumor/normal contrast of mammary metabolic rate of oxygen $[MMRO_{2(T/N)}]$ can be expressed as

$$MMRO_{2(T/N)} = \frac{saO_{2T} - svO_{2T}}{saO_{2N} - svO_{2N}} \frac{BF_T}{BF_N} = \frac{saO_{2T} - svO_{2T}}{saO_{2N} - svO_{2N}} \frac{BFI_T}{BFI_N}, \quad (7)$$

given the assumption that the changes of BFI are proportional to the changes of tissue blood flow (see Sec. 2.3). Assuming $saO_{2T} = saO_{2N} = 1$, we will have

$$\begin{aligned} MMRO_{2(T/N)} &= \frac{1 - svO_{2T}}{1 - svO_{2N}} \cdot \frac{BFI_T}{BFI_N} \\ &= \frac{(ctHHb_{vT}/ctTHb_{vT})}{(ctHHb_{vN}/ctTHb_{vN})} \frac{BFI_T}{BFI_N} \\ &= \left(\frac{ctHHb_{vT}}{ctHHb_{vN}} \frac{ctTHb_{vT}}{ctTHb_{vN}} \right)^{-1} \frac{BFI_T}{BFI_N}. \end{aligned} \quad (8)$$

The diffuse optical signal originates from the hemoglobin in the tissue within the view of the probe, and represents a mixture of arterial, capillary and venous blood. The mixed tissue compartment (MTC) viewed by the optical probe is a weighted average of the arterial (a), capillary (c), and venous (v) compartments, and the weight is proportional to the optical cross section of the corresponding compartment. For example, $ctHHb = k_1 \cdot ctHHb_a + k_2 \cdot ctHHb_c + k_3 \cdot ctHHb_v$, where k_1, k_2, and k_3 are the respective weights and $k_1 + k_2 + k_3 = 1$. If we further assume the quantities in the venous compartment are proportional to the MTC values, i.e.,

$$ctHHb_{vT} = r_{1T} \cdot ctHHb_T, ctTHb_{vT} = r_{2T} \cdot ctTHb_T,$$

$$ctHHb_{vN} = r_{1N} \cdot ctHHb_N, ctTHb_{vN} = r_{2N} \cdot ctTHb_N. \quad (9)$$

We can further simplify by defining $\gamma_{T(N)} = r_{1T(N)}/r_{2T(N)} = [ctHHb_{vT(N)}/ctHHb_{T(N)}]/[ctTHb_{vT(N)}/ctTHb_{T(N)}] = [ctHHb_{vT(N)}/ctTHb_{vT(N)}]/[ctHHb_{T(N)}/ctTHb_{T(N)}]$, which is the ratio of deoxy to total hemoglobin in the venous com-

partment compared to the ratio of deoxy to total hemoglobin in the total mixed vasculature. As a result, we will have

$$
\begin{aligned}
\mathrm{MMRO}_{2(T/N)} &= \frac{r_{1T} \cdot \mathrm{ctHHb}_T}{r_{1N} \cdot \mathrm{ctHHb}_N} \left(\frac{r_{2T} \cdot \mathrm{ctTHb}_T}{r_{2N} \cdot \mathrm{ctTHb}_N} \right)^{-1} \frac{\mathrm{BFI}_T}{\mathrm{BFI}_N} \\
&= \frac{r_{1T}/r_{2T}}{r_{1N}/r_{2N}} \frac{\mathrm{ctHHb}_T}{\mathrm{ctHHb}_N} \left(\frac{\mathrm{ctTHb}_T}{\mathrm{ctTHb}_N} \right)^{-1} \frac{\mathrm{BFI}_T}{\mathrm{BFI}_N} \\
&= \frac{\Gamma_T}{\Gamma_N} \frac{\mathrm{ctHHb}_T}{\mathrm{ctHHb}_N} \left(\frac{\mathrm{ctTHb}_T}{\mathrm{ctTHb}_N} \right)^{-1} \frac{\mathrm{BFI}_T}{\mathrm{BFI}_N},
\end{aligned}
\tag{10}
$$

where Γ_T and Γ_N are two unknowns. The ratio of Γ_T/Γ_N reflects the relative oxygen extraction ability of the vasculature. For example, a Γ_T/Γ_N ratio larger than 1 means a higher tumor deoxyhemoglobin fraction in the venous compartment relative to the total mixed vasculature compared to the normal tissue, reflecting a larger portion of oxygen is extracted from the tumor tissue.

Acknowledgments

References

1. B. W. Pogue, S. P. Poplack, T. O. McBride, W. A. Wells, K. S. Osterman, U. L. Osterberg, and K. D. Paulsen, "Quantitative hemoglobin tomography with diffuse near-infrared spectroscopy: pilot results in the breast," *Radiology* **218**(1), 261–266 (2001).
2. H. B. Jiang, N. V. Iftimia, Y. Xu, J. A. Eggert, L. L. Fajardo, and K. L. Klove, "Near-infrared optical imaging of the breast with model-based reconstruction," *Acad. Radiol.* **9**(2), 186–194 (2002).
3. A. Li, E. L. Miller, M. E. Kilmer, T. J. Brukilacchio, T. Chaves, J. Stott, Q. Zhang, T. Wu, M. Chorlton, R. H. Moore, D. B. Kopans, and D. A. Boas, "Tomographic optical breast imaging guided by three-dimensional mammography," *Appl. Opt.* **42**, 5181–5190 (2003).
4. B. Chance, S. Nioka, J. Zhang, E. F. Conant, E. Hwang, S. Briest, S. G. Orel, M. D. Schnall, and B. J. Czerniecki, "Breast cancer detection based on incremental biochemical and physiological properties of breast cancers: a six-year, two-site study," *Acad. Radiol.* **12**, 925–933 (2005).
5. C. H. Schmitz, D. P. Klemer, R. Hardin, M. S. Katz, Y. Pei, H. L. Graber, M. B. Levin, R. D. Levina, N. A. Fraco, W. B. Solomon, and R. L. Barbour, "Design and implementation of dynamic near-infrared optical tomographic imaging instrumentation for simultaneous dual-breast measurements," *Appl. Opt.* **44**, 2140–2153 (2005).
6. T. Yates, J. C. Hebden, A. Gibson, N. Everdell, S. R. Arridge, and M. Douek, "Optical tomography of the breast using a multi-channel time-resolved imager," *Phys. Med. Biol.* **50**(11), 2503–2518 (2005).
7. D. Grosenick, K. T. Moesta, M. Möller, J. Mucke, H. Wabnitz, B. Gebauer, C. Stroszczynski, B. Wassermann, P. M. Schlag, and H. Rinneberg, "Time-domain scanning optical mammography: I. Recording and assessment of mammograms of 154 patients," *Phys. Med. Biol.* **50**(11), 2429–2450 (2005).
8. D. Grosenick, H. Wabnitz, K. T. Moesta, J. Mucke, P. M. Schlag, and H. Rinneberg, "Time-domain scanning optical mammography: II. Optical properties and tissue parameters of 87 carcinomas," *Phys. Med. Biol.* **50**(11), 2451–2468 (2005).
9. X. Intes, "Time-Domain optical mammography SoftScan: initial results," *Acad. Radiol.* **12**, 934–947 (2005).
10. A. Cerussi, N. Shah, D. Hsiang, A. Durkin, J. Butler, and B. J. Tromberg, "In vivo absorption, scattering, and physiologic properties of 58 malignant breast tumors determined by broadband diffuse optical spectroscopy," *J. Biomed. Opt.* **11**(4), 044,005 (2006).
11. V. Ntziachristos, A. G. Yodh, M. D. Schnall, and B. Chance, "MRI-guided diffuse optical spectroscopy of malignant and benign breast lesions," *Neoplasia* **4**, 347–354 (2002).
12. H. Dehghani, B. W. Pogue, S. P. Poplack, and K. D. Paulsen, "Multiwavelength three-dimensional near-infrared tomography of the breast: initial simulation, phantom, and clinical results," *Appl. Opt.* **42**, 135–145 (2003).
13. Q. I. Zhu, M. M. Huang, N. G. Chen, K. Zarfos, B. Jagjivan, M. Kane, P. Hedge, and S. H. Kurtzman, "Ultrasound-guided optical tomographic imaging of malignant and benign breast lesions: initial clinical results of 19 cases," *Neoplasia* **5**(5), 379–388 (2003).
14. D. B. Jakubowski, A. E. Cerussi, F. Bevilacqua, N. Shah, D. Hsiang, J. Butler, and B. J. Tromberg, "Monitoring neoadjuvant chemotherapy in breast cancer using quantitative diffuse optical spectroscopy: a case study," *J. Biomed. Opt.* **9**(1), 230–238 (2004).
15. Q. N. Zhu, S. H. Kurtzman, P. Hegde, S. Tannenbaum, M. Kane, M. M. Huang, N. G. Chen, B. Jagjivan, and K. Zarfos, "Utilizing optical tomography with ultrasound localization to image heterogeneous hemoglobin distribution in large breast cancers," *Neoplasia* **7**(3), 263–270 (2005).
16. R. Choe, A. Corlu, K. Lee, T. Durduran, S. D. Konecky, M. Grosicka-Koptyra, S. R. Arridge, B. J. Czerniecki, D. L. Fraker, A. DeMichele, B. Chance, M. A. Rosen, and A. G. Yodh, "Diffuse optical tomography of breast cancer during neoadjuvant chemotherapy: a case study with comparison to MRI," *Med. Phys.* **32**(4), 1128–1139 (2005).
17. N. Shah, J. Gibbs, D. Wolverton, A. Cerussi, N. Hylton, and B. J. Tromberg, "Combined diffuse optical spectroscopy and contrast-enhanced magnetic resonance imaging for monitoring breast cancer neoadjuvant chemotherapy: a case study," *J. Biomed. Opt.* **10**(5), 051,503 (2005).
18. P. Taroni, A. Torricelli, L. Spinelli, A. Pifferi, F. Arpaia, G. Danesini, and R. Cubeddu, "Time-resolved optical mammography between 637 and 985 nm: clinical study on the detection and identification of breast lesions," *Phys. Med. Biol.* **50**(11), 2469–2488 (2005).
19. B. J. Tromberg, A. Cerussi, N. Shah, M. Compton, A. Durkin, D. Hsiang, J. Butler, and R. Mehta, "Imaging in breast cancer—diffuse optics in breast cancer: detecting tumors in pre-menopausal women and monitoring neoadjuvant chemotherapy," *Breast Cancer Res.* **7**(6), 279–285 (2005).
20. J. C. Hebden, T. D. Yates, A. Gibson, N. Everdell, S. R. Arridge, D. W. Chicken, M. Douek, and M. R. S. Keshtgar, "Monitoring recovery after laser surgery of the breast with optical tomography: a case study," *Appl. Opt.* **44**(10), 1898–1904 (2005).
21. E. Bombardieri, "Nuclear medicine applications for bone metastases—foreward," *Q. J. Nucl. Med.* **45**(1), 1–1 (2001).
22. G. Maret and P. Wolf, "Multiple light scattering from disordered media. The effect of Brownian motion of scatterers," *Z. Phys. B* **65**(4), 409–413 (1987).
23. D. Pine, D. Weitz, P. Chaikin, and Herbolzheimer, "Diffusing-wave spectroscopy," *Phys. Rev. Lett.* **60**, 1134–1137 (1988).
24. D. A. Boas, L. E. Campbell, and A. G. Yodh, "Scattering and Imaging with diffusing temporal field correlations," *Phys. Rev. Lett.* **75**(9), 1855–1858 (1995).
25. D. A. Boas and A. G. Yodh, "Spatially varying dynamical properties of turbid media probed with diffusing temporal light correlation," *J. Opt. Soc. Am. A* **14**(1), 192–215 (1997).
26. C. Cheung, J. P. Culver, K. Takahashi, J. H. Greenberg, and A. G. Yodh, "In vivo cerebrovascular measurement combining diffuse near-infrared absorption and correlation spectroscopies," *Phys. Med. Biol.* **46**(8), 2053–2065 (2001).
27. J. P. Culver, T. Durduran, T. Furuya, C. Cheung, J. H. Greenberg, and A. G. Yodh, "Diffuse optical tomography of cerebral blood flow, oxygenation, and metabolism in rat during focal ischemia," *J. Cereb. Blood Flow Metab.* **23**, 911–924 (2003).
28. T. Durduran, G. Q. Yu, M. G. Burnett, J. A. Detre, J. H. Greenberg, J. Wang, C. Zhou, and A. G. Yodh, "Diffuse optical measurement of blood flow blood oxygenation and metabolism in a human brain during sensorimotor cortex activation," *Opt. Lett.* **29**, 1766–1768 (2004).
29. J. Li, G. Dietsche, D. Iftime, S. E. Skipetrov, G. Maret, T. Elbert, B. Rockstroh, and T. Gisler, "Noninvasive detection of functional brain activity with near-infrared diffusing-wave spectroscopy," *J. Biomed.*

Opt. **10**(4), 1–12 (2005).

30. C. Zhou, G. Q. Yu, D. Furuya, J. H. Greenberg, A. G. Yodh, and T. Durduran, "Diffuse optical correlation tomography of cerebral blood flow during cortical spreading depression in rat brain," *Opt. Express* **14**, 1125–1144 (2006).

31. F. Jaillon, J. Li, G. Dietsche, T. Elbert, and T. Gisler, "Activity of the human visual cortex measured non-invasively by diffusing-wave spectroscopy," *Opt. Express* **15**, 6643–6650 (2007).

32. G. Q. Yu, T. Durduran, G. Lech, C. Zhou, B. Chance, R. E. Mohler, and A. G. Yodh, "Time-dependent blood flow and oxygenation in human skeletal muscles measured with noninvasive near-infrared diffuse optical spectroscopies," *J. Biomed. Opt.* **10**, 024027 (2005).

33. G. Q. Yu, T. Floyd, T. Durduran, C. Zhou, J. J. Wang, J. A. Detre, and A. G. Yodh, "Validation of diffuse correlation spectroscopy for muscle blood flow with concurrent arterial spin labeled perfusion MRI," *Opt. Express* **15**(3), 1064–1075 (2007).

34. G. Q. Yu, T. Durduran, C. Zhou, H. W. Wang, M. E. Putt, H. M. Saunders, C. M. Sehgal, E. Glatstein, A. G. Yodh, and T. M. Busch, "Noninvasive monitoring of murine tumor blood flow during and after photodynamic therapy provides early assessment of therapeutic efficacy," *Clin. Cancer Res.* **11**(9), 3543–3552 (2005).

35. G. Q. Yu, T. Durduran, C. Zhou, T. C. Zhu, J. C. Finlay, T. M. Busch, S. B. Malkowicz, S. M. Hahn, and A. G. Yodh, "Real-time in situ monitoring of human prostate photodynamic therapy with diffuse light," *Photochem. Photobiol.* **82**(5), 1279–1284 (2006).

36. U. Sunar, H. Quon, T. Durduran, J. Zhang, J. Du, C. Zhou, G. Q. Yu, R. Choe, A. Kilger, R. Lustig, L. Loevner, S. Nioka, B. Chance, and A. G. Yodh, "Noninvasive diffuse optical measurement of blood flow and blood oxygenation for monitoring radiation therapy in patients with head and neck tumors: a pilot study," *J. Biomed. Opt.* **11**, 064,021 (2006).

37. T. Durduran, R. Choe, G. Q. Yu, C. Zhou, J. C. Tchou, B. J. Czerniecki, and A. G. Yodh, "Diffuse optical measurement of blood flow in breast tumors," *Opt. Lett.* **30**, 2915–2917 (2005).

38. H. Madjar, W. Sauerbrei, H. J. Prompeler, R. Wolfarth, and H. Gufler, "Color Doppler and duplex flow analysis for classification of breast lesions," *Gynecol. Oncol.* **64**(3), 392–403 (1997).

39. D. A. Mankoff, L. K. Dunnwald, J. R. Gralow, G. K. Ellis, E. K. Schubert, J. Tseng, T. J. Lawton, H. M. Linden, and R. B. Livingston, "Changes in blood flow and metabolism in locally advanced breast cancer treated with neoadjuvant chemotherapy," *J. Nucl. Med.* **44**(11), 1806–1814 (2003).

40. J. P. Delille, P. J. Slaneta, E. D. Yeh, E. F. Halpern, D. B. Kopans, and L. Garrido, "Invasive ductal breast carcinoma response to neoadjuvant chemotherapy: noninvasive monitoring with functional MR imaging—pilot study," *Radiology* **228**(1), 63–69 (2003).

41. G. M. McDermott, A. Welch, R. T. Staff, F. J. Gilbert, L. Schweiger, S. I. Semple, T. A. Smith, A. W. Hutcheon, I. D. Miller, I. C. Smith, and S. D. Heys, "Monitoring primary breast cancer throughout chemotherapy using FDG-PET," *Breast Cancer Res. Treat.* **102**(1), 75–84 (2007).

42. C. Rousseau, A. Devillers, C. Sagan, L. Ferrer, B. Bridji, L. Campion, M. Ricaud, E. Bourbouloux, I. Doutriaux, M. Clouet, D. Berton-Rigaud, C. Bouriel, V. Delecroix, E. Garin, S. Rouquette, I. Resche, P. Kerbrat, J. F. Chatal, and M. Campone, "Monitoring of early response to neoadjuvant chemotherapy in stage II and III breast cancer by [18F]fluorodeoxyglucose positron emission tomography," *J. Clin. Oncol.* **24**(34), 5366–5372 (2006).

43. C. P. Chou, M. T. Wu, H. T. Chang, Y. S. Lo, H. B. Pan, H. Degani, and E. Furman-Haran, "Monitoring breast cancer response to neoadjuvant systemic chemotherapy using parametric contrast-enhanced MRI: a pilot study," *Acad. Radiol.* **14**(5), 561–573 (2007).

44. R. L. Wahl, K. R. Zasadny, G. D. Hytchins, M. Helvie, and R. Cody, "Metabolic monitoring of breast cancer chemohormonotherapy using positron emission tomography (PET): initial evaluation," *J. Clin. Oncol.* **11**, 2101–2111 (1993).

45. E. Bombardieri and F. Crippa, "PET imaging in breast cancer," *Q. J. Nucl. Med.* **45**(3), 245–255 (2001).

46. F. Bevilacqua, A. J. Berger, A. E. Cerussi, D. Jakubowski, and B. J. Tromberg, "Broadband absorption spectroscopy in turbid media by combined frequency-domain and steady-state methods," *Appl. Opt.* **39**(34), 6498–6507 (2000).

47. R. Graaff, J. G. Aarnoudse, J. R. Zijp, P. M. A. Sloot, F. F. M. de Mul, J. Greve, and M. H. Koelink, "Reduced light-scattering properties for mixtures of spherical particles: a simple approximation derived from Mie calculations," *Appl. Opt.* **31**(10), 1370–1376 (1992).

48. J. R. Mourant, T. Fuselier, J. Boyer, T. M. Johnson, and I. J. Bigio, "Predictions and measurements of scattering and absorption over broad wavelength ranges in tissue phantoms," *Appl. Opt.* **36**(4), 949–957 (1997).

49. J. M. Schmitt and G. Kumar, "Optical scattering properties of soft tissue: a discrete particle model," *Appl. Opt.* **37**(13), 2788–2797 (1998).

50. R. Zander and F. Mertzlufft, "Tentative recommendations on terminology and definitions in the respiratory physiology: resume of the ISOTT consensus session 1992, *Oxyg. Transp. Tiss.* **15**, 913–919 (1994).

51. S. Rice, "Mathematical analysis of random noise," in *Noise and Stochastic Processes*, N. Wax, ed., p. 133, Dover, New York (1954).

52. T. Durduran, "Noninvasive measurements of tissue hemodynamics with hybrid diffuse optical methods," Ph.D. Dissertions, University of Pennsylvania (2004).

53. A. Einstein, "On the motion of small particles suspended in liquids at rest required by the molecular-kinetic theory of heat," *Ann. Phys.* **17**, 549–560 (1905).

54. C. Menon, G. M. Polin, I. Prabakaran, A. Hsi, C. Cheung, J. P. Culver, J. F. Pingpank, C. S. Sehgal, A. G. Yodh, D. G. Buerk, and D. L. Fraker, "An integrated approach to measuring tumor oxygen status using human melanoma xenografts as a model," *Cancer Res.* **63**(21), 7232–7240 (2003).

55. F. Hyder, R. G. Shulman, and D. L. Rothman, "A model for the regulation of cerebral oxygen delivery," *J. Appl. Physiol.* **85**(2), 554–564 (1998).

56. R. D. Hoge, J. Atkinson, B. Gill, G. R. Crelier, S. Marrett, and G. B. Pike, "Investigation of BOLD signal dependence on cerebral blood flow and oxygen consumption: the deoxyhemoglobin dilution model," *Magn. Reson. Med.* **42**(5), 849–863 (1999).

57. J. B. Mandeville, J. J. Marota, C. Ayata, M. A. Moskowitz, R. M. Weisskoff, and B. R. Rosen, "MRI measurement of the temporal evolution of relative CMRO(2) during rat forepaw stimulation," *Magn. Reson. Med.* **42**(5), 944–951 (1999).

58. J. Mayhew, D. Johnston, J. Martindale, M. Jones, J. Berwick, and Y. Zheng, "Increased oxygen consumption following activation of brain: theoretical footnotes using spectroscopic data from barrel cortex," *Neuroimage* **13**(6), 975–987 (2001).

59. M. Jones, J. Berwick, D. Johnston, and J. Mayhew, "Concurrent optical imaging spectroscopy and laser-Doppler flowmetry: the relationship between blood flow, oxygenation, and volume in rodent barrel cortex," *Neuroimage* **13**(6, Pt 1), 1002–1015 (2001).

60. B. Ances, D. Wilson, J. Greenberg, and J. Detre, "Dynamic changes in cerebral blood flow, O_2 tension, and calculated cerebral metabolic rate of O_2 during functional activation using oxygen phosphorescence quenching," *J. Cereb. Blood Flow Metab.* **21**, 511–516 (2001).

61. D. A. Boas, G. Strangman, J. P. Culver, R. D. Hoge, G. Jasdzewski, R. A. Poldrack, B. R. Rosen, and J. B. Mandeville, "Can the cerebral metabolic rate of oxygen be estimated with near-infrared spectroscopy?" *Phys. Med. Biol.* **48**, 2405–2418 (2003).

62. A. Makris, T. J. Powles, S. Kakolyris, M. Dowsett, S. E. Ashley, and A. L. Harris, "Reduction in angiogenesis after neoadjuvant chemoendocrine therapy in patients with operable breast carcinoma," *Cancer* **85**(9), 1996–2000 (1999).

63. J. Tseng, L. K. Dunnwald, E. K. Schubert, J. M. Link, S. Minoshima, M. Muzi, and D. A. Mankoff, "F18-FDG kinetics in locally advanced breast cancer: correlation with tumor blood flow and changes in response to neoadjuvant chemotherapy," *J. Nucl. Med.* **45**(11), 1829–1837 (2003).

64. R. Johnson, "Thermodynamic method for investigation of radiation-induced changes in microcirculation of human tumors," *Int. J. Radiat. Oncol., Biol., Phys.* **1**, 659–670 (1976).

65. M. J. Mantyla, J. T. Toivanen, M. A. Pitkanen, and A. H. Rekonen, "Radiation-induced changes in regional blood flow in human tumors," *Int. J. Radiat. Oncol., Biol., Phys.* **8**(10), 1711–1717 (1982).

66. A. F. DeVries, C. Kremser, P. A. Hein, J. Griebel, A. Krezcy, D. Ofner, K. P. Pfeiffer, P. Lukas, and W. Judmaier, "Tumor microcirculation and diffusion predict therapy outcome for primary rectal carcinoma," *Int. J. Radiat. Oncol., Biol., Phys.* **56**(4), 958–965 (2003).

67. N. Shah, A. E. Cerussi, D. Jakubowski, D. Hsiang, J. Butler, and B. J. Tromberg, "The role of diffuse optical spectroscopy in the clinical management of breast cancer," *Dis. Markers* **19**, 95–105 (2003).

68. R. P. Beaney, A. A. Lammertsma, T. Jones, C. G. McKenzie, and K. E. Halnan, "Positron emission tomography for in-vivo measurement of regional blood flow, oxygen utilisation, and blood volume in patients with breast carcinoma," *Lancet* **1**, 131–134 (1984).

69. A. A. Lammertsma, "Positron emission tomography and in vivo measurements of tumour perfusion and oxygen utilisation," *Cancer Metastasis Rev.* **6**, 521–539 (1987).

70. P. Vaupel, F. Kallinowski, and P. Okunieff, "Blood flow, oxygen and nutrient supply, and metabolic microenvironment of human tumors: a review," *Cancer Res.* **49**(23), 6449–6465 (1989).

71. P. Vaupel and M. Hockel, "Blood supply, oxygenation status and metabolic micromilieu of breast cancers: characterization and therapeutic relevance (review)," *Int. J. Oncol.* **17**(5), 869–879 (2000).